OPTICAL AND STRUCTURAL PROPERTIES OF 100 MeV Ag SWIFT HEAVY ION IRRADIATED AMORPHOUS $Ge_{24}Se_{61}Sb_{15}$ THIN FILMS

S. PANDEY[*], R. CHAUHAN

Department of physics, D.A-V. College, C.S.J. M. University, Kanpur, Uttar Pradesh, India-208001

Present study reports about change in structural and linear/nonlinear optical properties of amorphous $Ge_{24}Se_{61}Sb_{15}$ thin films using 100 MeV silver (Ag) swift heavy ion (SHI) irradiation. The thin films were irradiated under 100 MeV Ag SHI for six different fluences ($3x10^{10}$, $1x10^{11}$, $3x10^{11}$, $1x10^{12}$, $3x10^{12}$, and $1x10^{13}$ ions/cm^2). The XRD images of the pristine and irradiated ($3x10^{12}$ ions/cm^2) thin films confirm the amorphous nature of thin films. The scanning electron microscopy (SEM) micrograph reveals that the fluence $1x10^{13}$ ions/cm^2 is the upper limit of ion fluence. The loss of energy and stopping range of 100 MeV Ag SHI was calculated using SRIM-2006. The electronic energy loss dominates over nuclear energy loss, hence is mainly responsible for optical and structural changes. The optical transmission spectra of the pristine and irradiated thin films were recorded within the spectral range from 300 nm to 900 nm. The optical absorption coefficient was calculated by using the Lambert-Beer law. The optical band gap (E_g) was calculated by extrapolating the Tauc's plot. The optical band gap (E_g) reduces from 1.59 eV (pristine) to 1.38 eV ($3x10^{12}$ ions/cm^2) and further increases to 1.48 eV ($1x10^{13}$ ions/cm^2). Linear and nonlinear refractive index were calculated using semi-empirical relations and both increases till fluence $3x10^{12}$ ions/cm^2, which is the consequence of bonding rearrangement as explained using Raman measurement.

1. Introduction

Chalcogenide glassy alloys (CGA) considered as technically important materials for optical and photonics applications. CGA has remarkable optical properties such as compositional-dependent optical band gap, ultrafast response time and higher linear/nonlinear refractive index than silica-based glasses [1]. In recent years, a new branch has been developed by the consortium of CGA and Photonics to formulate new applications as well as understand their basic-mechanisms. This new branch is named Chalcognide –Photonics (Ch-Phot) [2]. Due to limited optical properties, binary chalcogenide alloys were unable to meet the demand for Ch-Phot, so scientists began to be attracted toward the study of ternary-amorphous chalcogenide materials (TAC).

TAC has excellent transparency and high linear and non-linear refractive index in the infra-red range. The above property motivated to scientist use in the waveguide for all-optical processing of high-speed optical signals, optical phase-change memory, and a demultiplexer at high data rates [3-5].

TAC has a wider glass-forming region than the binary chalcogenides. Due to a variety of elements, TAC has higher glass transition temperature. High glass transition temperature makes them preferable material for optical and solid-state devices [6].

The chemical bonds rearrangement takes place within the TAC even in bulk or thin film form when treated with light, heat, energetic ions etc. This lead to a change in physical properties such as band gap, linear refractive index etc [7, 8]. The optical, electrical parameters change with

---

[*] Corresponding author: pandeys789@gmail.com

the thickness of the thin film. Parameters also are changed according to the determination technique or method. The physical properties of the TAC can be modified by an increase/decrease of the atomic percentage of one or more than one elements [9]. Heat treatment (thermal annealing) causes phase transformation as well as increase or decrease in the optical parameters of the TAC. So TAC can be used for phase-change memory and optical recording applications [10]. Energetic ion beam (Swift heavy ions) changes the optical and structural properties of TAC in a different route. Changes in properties of target material depend upon the energy, mass, and fluence of the energetic ion species. The ion beam is irradiated on the limited area of the thin film surface. So the properties of the materials change in the irradiated area and related volume below the surface only [11].

Ge-Se-Sb glass is environmental friendly and safe in comparison to As based TAC because of the absence of toxic element As. Sb and As both are metals but Sb has more metallic character than As. Sb has a higher atomic number, atomic weight and larger atomic radius so it can be expected that Ge-Se-Sb will have higher nonlinearity. Hence Ge-Se-Sb can be used in fabricating waveguide for high-speed optical signal processing and ultrafast all-optical switches etc.

In this paper, optical and structural properties are modified using 100 MeV silver (Ag) swift heavy ion (SHI) irradiation technique in amorphous $Ge_{24}Se_{61}Sb_{15}$ thin films for passive and active optical applications, waveguide, all-optical processing. $Ge_{24}Se_{61}Sb_{15}$ thin films were irradiated by 100 MeV Silver (Ag) swift heavy ions (SHI) for six different fluences ($3x10^{10}$, $1x10^{11}$, $3x10^{11}$, $1x10^{12}$, $3x10^{12}$, and $1x10^{13}$ ions/cm^2).

2. Experimental

For glass ($Ge_{30}Se_{58}Sb_{12}$) formation, a very reliable and conventional (melt-quenching) technique was utilized. These elements (99.999% pure germanium, selenium, and antimony) were weighted according to their atomic percentage then filled and sealed in a quartz ampoule at base pressure $1x10^{-5}$ mbar. This sealed ampoule was placed inside a rocking furnace then heated up to 950^oC at a rate of $3-4^oC$ / min for 10 hours to make homogeneous-melt.After completing the above process, this ampoule was quenched in ice water then the glass was taken out after breaking the quartz ampoule. The thin films were deposited on the soda-lime glass substrate by frequently used thermal evaporation technique. The soda-lime glass substrates were thoroughly cleaned twice using acetone, then dried properly. All procedures performed by wearing powder-free gloves.At base pressure $3x10^{-5}$ mbar, thin films were deposited at room temperature, inside the coating unit (HIND-HIVAC Model 12A 4DT).Target glass was placed into the small molybdenum vessel; the current pass through the vessel was 4.5 amperes for 12 seconds. Thickness profilometer (Tencore Instrument Model Alpha Step 100) was used to measure the thickness of the thin film. The amorphous nature of the bulk sample and thin films was determined by X-ray diffraction measurement (Hecus X-Ray Systems GmbH Model S3) with Cu Kα radiation.The SEM images (MIRA II LMH from TESCAN) and EDX (INCA PentaFET3) data was recorded by a Scanning Electron Microscope. The EDX data shows that the composition of thin-film was $Ge_{24.45}Se_{60.52}Sb_{15.04}$, which assumed to be $Ge_{24}Se_{61}Sb_{15}$.Thin films were exposed to swift heavy ions (SHI) of 100 MeV (Ag) energy in a 15 UD Pelletron tandem accelerator at IUAC in New Delhi. Thin films with an area of 1x1 cm^2 were exposed to SHI irradiation of six different fluences ($3x10^{10}$, $1x10^{11}$, $3x10^{11}$, $1x10^{12}$, $3x10^{12}$, and $1x10^{13}$ ions/cm^2).At room temperature, micro Raman data was recorded by a spectrometer (WITec GmbH Model Alpha 300) using a 514.4 nm argon ion laser (power density 5 mW / cm^2). The optical transmission spectra for normal incidence was recorded by double beam UV/Vis/IR computerized spectrophotometer (HITACHI Model UV 3300) in the wavelength range 300 – 900 nm.

3. Result and discussion

3.1. Loss of Energy and Stopping Range of Ions

Electronic-energy loss, nuclear-energy loss, stopping-range of 100 MeV silver (Ag) SHI irradiated ions in $Ge_{24}Se_{61}Sb_{15}$ thin-film was calculated by using SRIM 2006 [12]. The calculation showed that electronic-energy loss of ions in the thin film was 1.435×10^3 eV/Å, and nuclear energy loss was 9.372 eV/Å. The electronic-energy loss was 153 times higher than nuclear energy loss. So in this case, 100 MeV Ag SHI irradiation electronic-energy losses are mainly responsible for modification in properties of the material. The stopping-range of 100 MeV Ag SHI for this thin film was 12.89 μm which was more than the thickness of the thin film (1.19 μm), so irradiated ions come into rest in soda-lime glass substrate after passing through the thin film.

3.2. XRD Measurement

For the structural study of thin films material, the X-ray diffraction technique has used. X-ray micrographs of pristine and 100 MeV Ag SHI irradiated (1×10^{13} ions/cm^2) thin-film are shown in Fig. 1. Looking closely at the diffraction pattern of pristine and irradiated thin film, it was found that no sharp peaks are present in them. The nature of the thin film reveals that it is amorphous. The resulting 100 MeV silver (Ag) SHI radiation causes no phase change and thethin films maintained an amorphous nature.
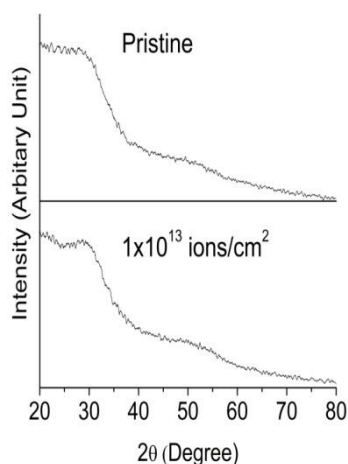

Fig. 1.XRD images of pristine and irradiated ($1x10^{13}$ ions/cm^2) thin film.

3.3. SEM Analysis

Scanning electron microscopy (SEM) images of the pristine and 100 MeV Ag ions irradiated (1×10^{13} ions/cm^2) thin film are shown in Fig. 2. The surface of the pristine thin-film looks smooth, whereas bright particles are observed at several spots. A large number of cracks and bubbles are observed on the surface of the irradiated thin film. Surface morphology of irradiated thin-film indicates that fluence1×10^{13} ions/cm^2 causes surface destruction to thin film. It indicates that the upper limit of fluence, which can be used for the treatment of thin films, is below the fluence1×10^{13} ions/cm^2.
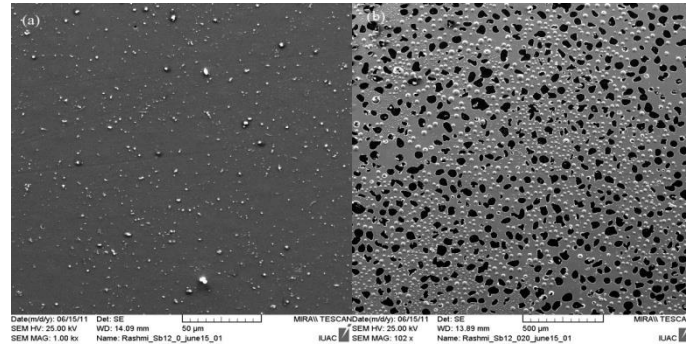
Fig. 2.SEM images of (a) Pristine and (b) Irradiated ($1x10^{13}$ ions/cm^2) thin films.

3.4. Optical Analysis

The optical transmission spectra of pristine and irradiated thin films in the spectral range from 500 nm up to 900 nm are shown in Figure 3. Due to the limited thickness of few thin films, the optical interference fringes do not form properly. Therefore the coefficient of optical absorption has calculated by Lambert-Beer law.

$$\alpha = \frac{1}{d}\log_e\left(\frac{1}{T}\right) \tag{1}$$

Where d is the thickness of thin film and T is the optical transmission.

Coefficient of absorption has shown in Table I. it is a measurement of the fraction of absorbed energy by the transparent medium to the total energy incident on the surface. The coefficient of absorption for the pristine thin film is 3960 cm^{-1}. The ion irradiation causes an increment in the optical absorption coefficient. Due to ion irradiation, the coefficient of absorption has increased to 10133 cm^{-1} till fluence$1x10^{12}$ ion/cm^2. Thereafter it has reduced to 6403 cm^{-1} till fluence$3x10^{12}$ ions/cm^2.

The optical band gap has calculated by the method those described by Tauc by extrapolating the Tauc's plot for indirect bandgap material [13].

$$\sqrt{\alpha h\nu} = \sqrt{B}\left(h\nu - E_g\right) \tag{2}$$

where, $B^{1/2}$ is the Tauc's parameter which measures the disorder of the material. The value $B^{1/2}$ is expressed by the slope of the absorption edge, where $\alpha \geq 10^4$ cm^{-1}.Calculated values of the optical band gap have shown in Fig. 4, and Table 1. Calculated valueof the optical band gap for the pristine thin film was 1.59 eV. The ion irradiation (100 MeV Ag SHI) has reduced the optical band gap to 1.38 eV till fluence $3x10^{12}$ ions/cm^2. After that ion irradiation has increased the optical band gap to 1.48 eV till fluence $1x10^{13}$ ions/cm^2.

Tauc's parameter ($B^{1/2}$) is the inverse measurement of the disorder. Increasing values of $B^{1/2}$ is an indication of a reduction in disorder. Similarly, a decrease in $B^{1/2}$ is the consequence of an increment in disorder. The value of Tauc's parameter for pristine thin film is 752.51. Ion irradiation till fluence $3x10^{12}$ ions/cm^{2}has decreased this value to 407.05. Further, the value has increased to 523.45 for fluence $1x10^{13}$ ions/cm^2.
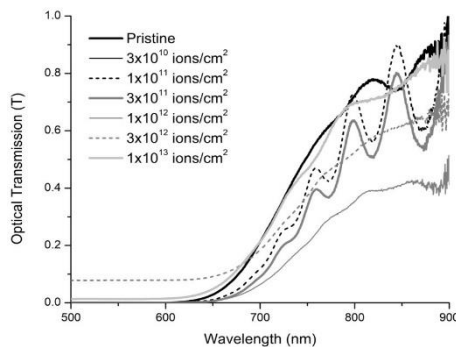
Fig. 3.Optical transmission spectra of pristine and irradiated thin films.

The static refractive index (n_o) has calculated by using the Dimitrov-Sakka formula from the optical band gap [14]

$$\frac{n_o^2-1}{n_0^2+2} = 1 - \left(\frac{E_g}{20}\right)^{1/2} \tag{3}$$

The static refractive index (n_o) of the pristine thin film is 2.94. Ion irradiation changes the static refractive index; hence it has increased to 3.07 tillfluence 3×10^{12} ions/cm^2. Thereafter it has reduced to 3.00 atfluence 1×10^{13} ions/cm^{2}as shown in Table I.

The degree of polarization is often shown by the linear optical susceptibility ($\chi^{(1)}$). The linear optical susceptibility is estimated using the semi-empirical formula. This formula is reported by Ticha and Tichy [15]

$$\chi^{(1)} = \frac{n_o^2-1}{4\pi} \tag{4}$$

The linear optical susceptibility of irradiated thin films increased from 0.608 to 0.670 till fluence 3×10^{12} ions/cm^2, after that decreased to 0.639 forfluence1×10^{13} ions/cm^2. Calculated values of the linear optical susceptibility are shown in Table I.

When the electromagnetic radiation is incident on the optical medium, then optical absorption and scattering phenomena happen; as a result attenuation of light signals in the optical medium takes place. The magnitude of attenuation of light signals in the optical medium is estimated by the following formula

$$k = \frac{\alpha\lambda}{4\pi} \tag{5}$$

The attenuation in the light signals has expressed by the extinction coefficient. Ion irradiation increased the extinction coefficient from 0.024 to 0.062 till fluence 1×10^{12} ions/cm^2. After that extinction coefficient decreased to 0.039 till fluence 3×10^{12} ions/cm^2. Values of the extinction coefficient are shown in Table 1.

Polarization is closely related to the first, second and third-order susceptibility. The nonlinear optical phenomena are majorly related to the third-order susceptibility. The third order nonlinear susceptibility ($\chi^{(3)}$) is determined by the Miller's rule [15]

$$\chi^{(3)} = \frac{A}{(4\pi)^2} (n_o^2 - 1)^4 \tag{6}$$

where$A = 1.7\times10^{-10}$ [esu]

The ion irradiation has increased the third-order nonlinear susceptibility from 2.32×10^{-11} [esu] to 3.42×10^{-11} [esu] till fluence 3×10^{12} ions/cm^2. Thereafter the third-order susceptibility decreased to 2.83×10^{-11} [esu] for fluence 1×10^{13} ions/cm^2.

While designing the optical and photonic devices, the nonlinear index of refraction plays a crucial role. The nonlinear index of refraction is determined by the semi-empirical formula using the optical band gap [15]

$$n_2[esu] \sim \frac{\check{A}}{E_g^4} \qquad (7)$$

where $\check{A} = 1.26 \times 10^{-9}$ [esu(eV)^4]

Due to the effect of ion irradiation, the nonlinear index of refraction increased from 1.97×10^{-10} [esu(eV)^4] to 3.47×10^{-10} [esu(eV)^4] till fluence 3×10^{12} ions/cm^2, then decreased to 2.63×10^{-10} [esu(eV)^4] for fluence 1×10^{13} ions/cm^2. The third-order nonlinear susceptibility and nonlinear index of refraction has shown in Table 1.
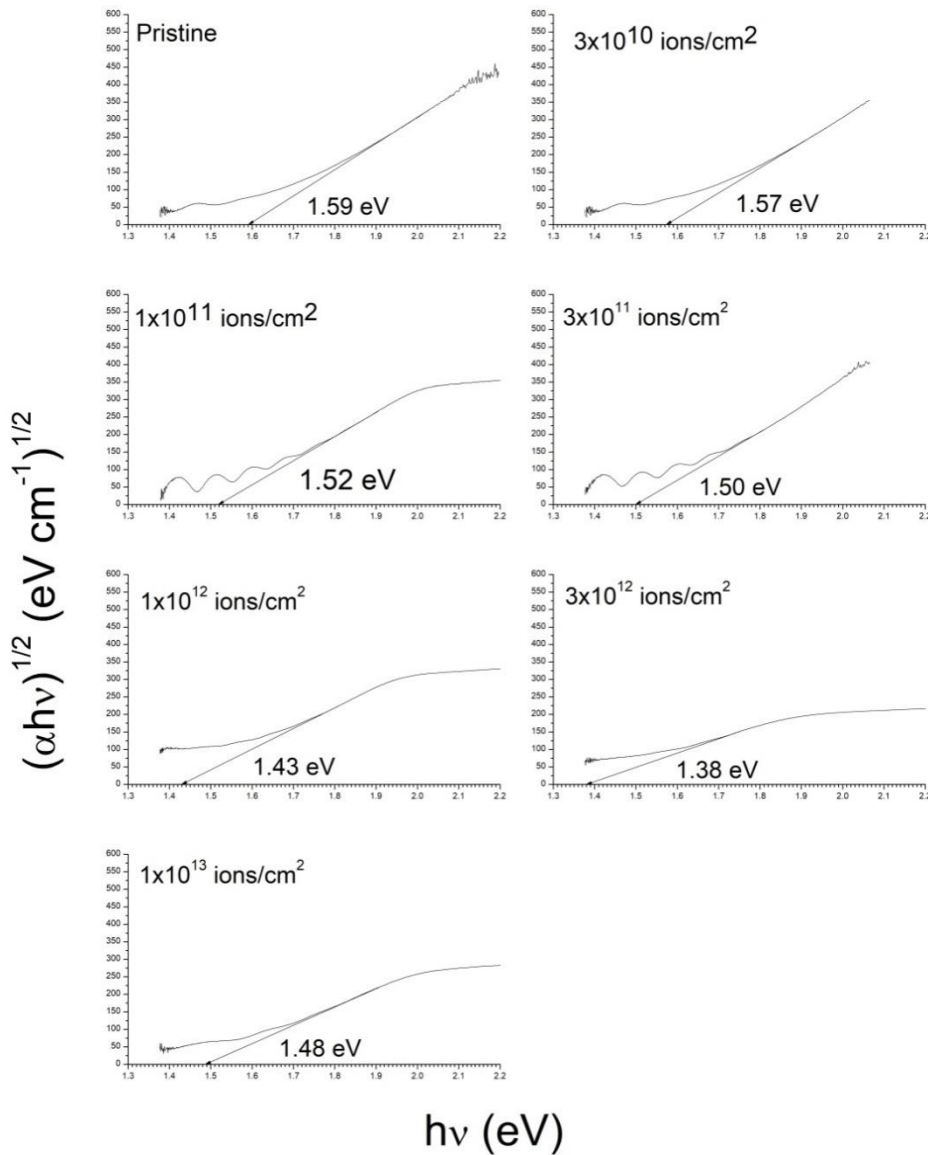

Fig.4.Optical band gap for pristine and irradiated thin films.

Due to the presence of short-range orders in chalcogenide glasses, the localized states are generated. External treatment techniques (light soaking, e-beam, laser irradiation, ion irradiation etc.) can narrow or broaden the localized states. Among these treatment techniques, the ion irradiation emerges as a very effective technique. Ion irradiation suddenly accumulates a large

amount of energy in the material. This accumulated energy generates ion tracks and defects in the material. Consequently, the dislocations increase in the material. The generated defects modify the tails of the material hence the width of localized states increased. This effect of broadening the localized states is observed on the values of Tauc's parameter and the optical band gap [16]. Therefore, Tauc's parameter ($B^{1/2}$) decreased due to increment in dislocation (disorder) in the material with increase in the fluence of ion irradiation. A similar trend is observed in the optical band gap because of the width of localized states increased and number of homopolar bonds increased. The ion irradiation increases the density of material, therefore the static index of refraction increased. Due to similar reason first and third order susceptibility, nonlinear index of refraction increased. This fact explained later in Raman analysis. But due to increasing values of extinction coefficient, this irradiated material may have limited use for the telecom applications.

Table 1.Band gap and other optical constant for pristine and irradiated thin films.

Fluence	α (cm^{-1}) at 775 nm	E_g (eV)	$B^{1/2}$	n_o	$\chi^{(1)}$	K at 775 nm	$\chi^{(3)}$ (10^{-13}esu)	n_2 (10^{-10}esu)
Pristine	3960	1.59	752.51	2.94	0.608	0.024	232.25	1.97
3×10^{10} ions/cm^2	3960	1.57	714.37	2.95	0.613	0.024	240.58	2.07
1×10^{11} ions/cm^2	7125	1.52	688.92	2.98	0.627	0.044	263.14	2.36
3×10^{11} ions/cm^2	8249	1.50	688.00	2.99	0.633	0.051	272.93	2.49
1×10^{12} ions/cm^2	10133	1.43	589.57	3.04	0.654	0.062	311.14	3.01
3×10^{12} ions/cm^2	6403	1.38	407.08	3.07	0.670	0.039	342.79	3.47
1×10^{13} ions/cm^2	10017	1.48	523.45	3.00	0.636	0.062	283.20	2.63

3.5. Raman Analysis

Raman investigations are helpful in understanding the structural changes occur in thin film samples due to external treatments [17, 18]. The microstructural changes in $Ge_{24}Se_{61}Sb_{15}$ thin film caused by (100 MeV Ag) SHI irradiation as revealed from Raman spectra are shown in Figure 5.Raman peak fitting figure of the pristine thin film exhibited peaks at 170 cm^{-1} (peak I), 196 cm^{-1} (peak II), and 217 cm^{-1} (peak III). Ion irradiation (100 MeV Ag SHI) shifted these peaks to 180 cm^{-1} (peak I), 201 cm^{-1} (peak II), and 219 cm^{-1} (peak III). It indicates that not any new bond formation is caused due to ion irradiation.

The first peak at 170 cm^{-1}in the pristine thin film is a contribution of stretching vibrations of Sb-Sb bonds in $Se_2Sb-SbSe_2$ structural units and stretching vibration modes of the Ge-Ge bonds in $Ge_2Se_{6/2}$ structural units [19-21].Gurey et al. found first peak in $Ge_{28}Se_{60}Sb_{12}$ glass at 160 cm^{-1} [19]. In the present sample, antimony is over-stoichiometry and germanium under-stoichiometry from the reference samples. Hence, in the present sample, the peak is found at 170 cm^{-1}.

The peak at 198 cm^{-1} in the pristine thin film originates due to the contribution of stretching mode of Sb-Se bond in $SbSe_{3/2}$ pyramidal units and stretching mode of Ge-Se bond in corner-sharing $GeSe_{4/2}$ tetrahedral units. Sb-Se bond in $SbSe_{3/2}$ pyramidal units is similar to the one reported in $Ge_{28}Se_{60}Sb_{12}$ glass at 200 cm^{-1}[19]. Ge-Se bond in corner-sharing $GeSe_{4/2}$ tetrahedral units is similar in a-$Ge_{21.5}Se_{78.5}$ sample [22, 23].

In accordance with previous studies, the peak at 217 cm^{-1} in the pristine thin film originates due to the A^c_1 breathing vibrations mode of Ge-Se bond in edge-sharing $Ge_2Se_2Se_{4/2}$bitetrahedral units and vibrations of Se atoms in edge-sharing $GeSe_{4/2}$ tetrahedral unit. Naik et al. reported similar to Ge-Se edge-sharing bond at 215 cm^{-1} in $Ge_{12}Se_{63}Sb_{25}$ thin film [24]. Dwivedi et al. reported similar bond at 215 cm^{-1} [22].

Due to high electronic energy loss (1.435×10^3 eV/Å), the ion irradiation not only changed the area under the peak and width but also shifted the peak position. Under the effect of 100 MeV Ag SHI irradiation (3×10^{12} ions/cm^2), the relative area under the peak 170 cm^{-1} increased from 0.361 to 0.620. The relative area under the peak 196 cm^{-1} decreased from 0.534 to 0.293. Similarly the relative area under the peak 217 cm^{-1} decreased from 0.105 to 0.087.

Change in relative area indicates that ion irradiation converts hetropolar Ge-Se, Sb-Se bonds into homopolar Ge-Ge, Sb-Sb bonds. The width of the peak at 170 cm^{-1} increased from 29.60 to 36.87. It indicates that ion irradiation increased disorder in thin film. Therefore, the optical band gap decreased.

Effect of ion irradiation (100 MeV Ag SHI) on the present film is different in nature because homopolar bonds increased. But it is expected that ion irradiation causes densification in the material. Hence, statistic refractive index, nonlinear refractive index, first and third order susceptibility of ion irradiated thin film increased.
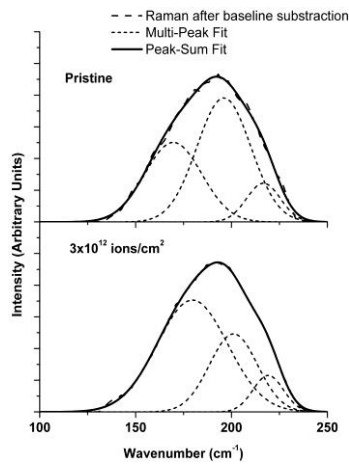

Fig.5. Raman peaks of pristine and irradiated ($3x10^{12}$ ions/cm^2) thin films.

Table 2. Raman peak details of pristine and irradiated thin films.

Peak details	Pristine			Irradiated (3×10^{12} ions/cm^2)		
	Peak position	Width	Relative Area	Peak position	Width	Relative Area
Stretching vibrations of Sb-Sb bonds in Se$_2$Sb-SbSe$_2$ molecular unit [19] and stretching vibrations mode of Ge-Ge bonds in GeSe$_{6/2}$ structural units [20, 21]	170	29.60	0.361	180	36.87	0.620
Sb-Se stretching modes in SbSe$_{3/2}$ pyramidal units [19] and stretching mode of Ge-Se bonds in corner sharing GeSe$_{4/2}$ tetrahedral unit [22, 23]	196	28.14	0.534	201	25.01	0.293
A$^c_1$ breathing vibration of Ge-Se bond in edge-sharing Ge$_2$Se$_2$Se$_{4/2}$ bitetrahedral units and vibrations of Se atoms in edge-shared GeSe$_{4/2}$ tetrahedral units [22, 24]	217	17.66	0.105	219	15.85	0.087

4. Conclusions

The following changes have been observed in amorphous Ge$_{24}$Se$_{61}$Sb$_{15}$ thin films under 100 MeV Ag SHI irradiation:

No crystallization is observed due to ion irradiation in and amorphous phase is found to be retained. Scanning Electron Microscope investigation shows cracks and bubbles formed at the surface of thin film irradiated at fluence1×10^{13} ions/cm^2. This finding indicates that the treatment of the thin films needs to be kept below 1×10^{13} ions/cm^2.

The optical band gap has decreased upon increasing ion fluence. Raman analysis revealed that destruction of GeSe$_{4/2}$ corner-sharing, edge-sharing, bitetrahedral, SbSe$_{3/2}$ pyramidal unit and increasing the homopolar bonds, which is responsible for reduction in optical band gap. The static refractive index, first and third-order susceptibility, and nonlinear refractive index has maximized at fluence 3×10^{12} ions/cm^2, after which these parameter values decrease as the fluence increases.

Ion irradiation has increased the density of the material, which is responsible for the increase of the linear/nonlinear susceptibility and linear/nonlinear refractive index. The present study helps to understand the influence of 100 MeV Ag SHI irradiation on optical/structural properties of amorphous Ge$_{24}$Se$_{61}$Sb$_{15}$ composition. The present study can be utilized for updating the treatment protocols where ion irradiations are applied over covalently bonded glasses to fabricate optical/photonic components for exalted performance.

Acknowledgements

References

[1] M. Olivier, J. C. Tchahame, P. Nemec, M. Chauvet, V. Besse, C. Cassagne, G. Boudebs, G. Renversez, R. Boidin, E. Baudet, V. Nazabal, Opt. Mater. Express **4**(3), 525 (2014).

[2] B. J. Eggleton, B. Luther-Davies, K. Richardson, Nat. Photonics **5**, 141 (2011).

[3] A. Prasad, C. Zha, R. Wang, A, Smith, A. Madden, B. Luther-Davies, Opt. Express **16**(4), 280408).

[4] T. Wang, X. Gai, W. Wei, R. Wang, Z, Yang, X. Shen, S. Madden, B. Luther-Davies, Opt. Mater.Express **4**(5), 1011 (2014).

[5] G. Demetriou, J. Bérubé, R. Vallée, Y. Messaddeq, C. Petersen, D. Jain, O. Bang, C. Craig, D. Hewak, A. Kar, Opt. Express **24**(6), 6350 (2016).

[6] D. A. P. Bulla, R. P. Wang, A. Prasad, A. V, Rode, S. J. Madden, B. Luther-Davies, Appl. Phys. A: Mater. Sci. Process. **96**, 615 (2009).

[7] Z. Zhang, S. Xu, X. Sneh, R. Wang, Opt. Mater.Express **10**(2), 540 (2020).

[8] M. Behera, N. C. Mishra, S. A. Khan, R. Naik, J. Non-Cryst. Solids **544**, 120191 (2020).

[9] M. Fadel, Vacuum **44**(8), 851 (1993).

[10] P. Nèmec, A. Moreac, V. Nazabal, M. Pavlišta, J. Přikryl, M. Frumar, J. Appl. Phys. **106**, 103509 (2009).

[11] R. Chauhan, A. Tripathi, A. K. Srivastava, K. K. Srivastava Chalcogenide Lett. **10**(2), 63 2013).

[12] J. F. Ziegler, SRIM 2006 Available from http://www.srim.org (last retrieved on April 30 2019).

[13] Optical Properties of Amorphous Semiconductors, J. Tauc: Amorphous and Liquid Semiconductors, Ed J. Tauc, Plenum Press, London and New York, 159 (1974).

[14] V. Dimitrov, S. Sakka, J. Appl. Phys. **79**(3), 1741 (1996).

[15] H. Tichá, L. Tichý, J. Opt. Adv. Mater**4**(2), 351 (2002).

[16] E. A. Davis, N. F. Mott, Electronic processes in non-crystalline materials, Clarendon, Oxford (1974).

[17] R. Chauhan, J. Non-oxide Glasses, **7**(3), 45 (2015).

[18] R. Chauhan, S. Pandey, S. G. Prasad, Chalcogenide Lett. **15**(5), 267 (2018).

[19] G. Guery, J. D. Musgraves, C. Labrugere, E. Fargin, T. Cardinal, and K. Richardson, J. Non-Cryst.Solids, **358**, 1740 (2012).

[20] I. Watanabe, S. Noguchi, T. Simizu J. Non-Cryst. Solids **58**, 35 (1983).

[21] V. Nazabal, F. Carpentier, J. Adam, P. Nemec, H. Lhermite, M, Brandily-Anne, J. Charrier, J. Guin, A. Morèac, Int. J. Appl. Ceram. Technol. **8**(5), 990 (2011).

[22] P. K. Dwivedi, S. K. Tripathi, A. Pradhan, V. N. Kulkarni, S. C. Agarwal, J. Non-Cryst. Solids **266-269**, 924 (2000).

[23] K. Jackson, A. Briley, S. Grossman, D. V. Porezag, M. R. Pederson, Phys. Rev. B **60**, R14985 (1999).

[24] R. Naik, S. Jena, R. Ganeshan, N. K. Sahoo, Indian J. Phys. **89**, 1031 (2015).